Title: Mutations of the serine protease CAP1/Prss8 lead to reduced embryonic viability, skin defects, and decreased ENaC activity.
Authors: Frateschi S, Keppner A, Malsure S, Iwaszkiewicz J, Sergi C, Merillat AM, Fowler-Jaeger N, Randrianarison N, Planès C, Hummler E
Journal: The American journal of pathology
Year: 2012 Aug
Volume: 181
Issue: 2
Pages: 605-15
DOI: 10.1016/j.ajpath.2012.05.007

"Mutations of the serine protease *CAP1/Prss8* lead to reduced embryonic viability, skin defects and decreased ENaC activity"

[1]Simona Frateschi, [1]Anna Keppner, [1]Sumedha Malsure, [2]Justyna Iwaszkiewicz, [1]Chloé Sergi, [1]Anne-Marie Merillat, [1]Nicole Fowler-Jaeger, [3]Nadia Randrianarison, [3]Carole Planès and [1]Edith Hummler.

[1]Department of Pharmacology and Toxicology, University of Lausanne, 1005 Lausanne, Switzerland

[2]Protein Modeling Facility, University of Lausanne, 1015 Lausanne, Switzerland

[3]EA2363, Université Paris 13, PRES Sorbonne Paris Cité F-93017 Bobigny, France.

Number of text pages, tables and figures: 29 pages, 1 table, 6 figures

Running head: *CAP1/Prss8* mutations lead to inheritance and skin defects *in vivo*.

Grant number and source of support: This work was supported by the Swiss National Science Foundation (Grant 3100A0-102125/1 to E. Hummler), the Swiss National Centre of Competence in Research (NCCR) Kidney Control of Homeostasis (Kidney.CH), and the Leducq Fondation.

Corresponding author: Edith Hummler; Département de Pharmacologie et de Toxicologie, Rue du Bugnon 27, CH-1005 Lausanne, Switzerland; Phone: +41/21-692 5357; Fax: +41/21-692 5355; e-mail: Edith.Hummler@unil.ch

Keywords: channel-activating protease 1 / prostasin / mouse and rat models /epithelial sodium channel (ENaC)

ABSTRACT

CAP1/Prss8 is a membrane-bound serine protease involved in the regulation of several different effectors, such as the epithelial sodium channel ENaC, the protease-activated receptor PAR2, the tight junction proteins and the profilaggrin polypeptide. Recently, the V170D and the G54-P57 deletion mutations within the *CAP1/Prss8* gene, identified in 'frizzy' mice (*fr*) and 'hairless' rats (fr^{CR}) respectively, have been proposed as causative of their skin phenotypes. In the present study, we analyzed those mutations revealing a change in the protein structure, a modification of the glycosylation state, and an overall reduction in the activation of ENaC of the two mutant proteins. *In vivo* analyses demonstrated that both *fr* and fr^{CR} mutant animals present analogous reduction of embryonic viability, similar histological aberrations at the level of the skin, and a significant decrease in the activity of ENaC in the distal colon in comparison with their control littermates. 'hairless' rats additionally showed dehydration defects in skin and intestine and significant reduction in the body weight. In conclusion, we provided molecular and functional evidences that *CAP1/Prss8* mutations are accountable for the defects in *fr* and fr^{CR} animals, and we furthermore demonstrated a decreased function of the CAP1/Prss8 mutant proteins. Therefore, *fr* and fr^{CR} animals emerged as suitable models to investigate the consequences of CAP1/Prss8 action on its target proteins in the whole organism.

INTRODUCTION

Proteolytic enzymes and their inhibitors count up for more than 2% of the known proteome and a crucial role of these proteins in tissue homeostasis, diseases and development is well demonstrated [1,2,3,4].

CAP1/Prss8 (also known as prostasin) is a glycosyl-phosphatidylinositol membrane-anchored serine protease expressed in the epithelium of various organs, such as prostate, kidney, lung, colon and skin [5,6,7]. CAP1/Prss8 was the first of several membrane-tethered serine proteases found to activate the amiloride-sensitive epithelial sodium channel ENaC in a kidney epithelial cell line, and for this reason it was named channel-activating protease 1 (CAP1) [8,9]. These findings predicted that CAP1/Prss8 has an important role in regulating the epithelial sodium transport *in vivo* [10], and ENaC currents became a suitable parameter to monitor CAP1/Prss8 activity.

CAP1/Prss8 has also been demonstrated to play essential functions in the physiopathology of lung and skin. *CAP1/Prss8* inactivation addressed to the alveolar epithelium decreased ENaC-mediated alveolar sodium transport, and increased alveolar lining fluid volume in an experimental model of acute volume-overload [6]. The lack of *CAP1/Prss8* in the skin caused early postnatal mortality because of severe skin dehydration defects, altered the processing of profilaggrin and generated defective tight junctions [7]. On the other hand, *CAP1/Prss8* overexpression in the skin severely impaired the epidermal barrier function and provoked ichthyosis and inflammation. Those pathological features were completely negated when superposed on a protease-activated receptor 2 (*PAR2*) knock-out background, placing PAR2 as a downstream effector of CAP1/Prss8 [1]. PAR2 is a G-protein-coupled receptor also involved in neural tube closure and it can be activated by local proteases as CAP1/Prss8 for regulating epithelial integrity [11]. Moreover, *CAP1/Prss8* was found down-regulated in hormone refractory prostate cancers, gastric and breast cancer [12,13,14], and up-regulated in

epithelial ovarian cancer [15], suggesting an additional role of CAP1/Prss8 in tumor invasion. Thus, CAP1/Prss8 emerged as involved in various different processes that range from organ integrity to disease.

Very recently, Spacek and colleagues located the genetic defects in the spontaneous 'frizzy' mouse (*fr*) and 'hairless' rat (fr^{CR}) models on the *CAP1/Prss8* gene [16]. Mice carrying the *fr* mutation in homozygosity display a nearly normal, wavy coat, and distinctly curly vibrissae that are apparent after birth and persist throughout life [17]. The Charles River 'hairless' rat fr^{CR} is one of the autosomal recessive hypotrichotic models actively studied in pharmacologic and dermatologic research, and it is characterized by almost complete baldness [18]. Spacek and coworkers demonstrated that the *fr* mutation consists of a T to A transversion in the *CAP1/Prss8* gene that results in a valine to aspartate substitution at residue 170. The assignment of *fr* mutation on the *CAP1/Prss8* gene was supported by complementation test that indicated the failure of the knock-out allele (Δ) of *CAP1/Prss8* [19] to complement the *fr* defect in compound heterozygotes (fr/Δ). In addition, sequence analysis of CAP1/Prss8 coding regions in the 'hairless' fr^{CR} rat identified a 12-bp deletion in the third exon leading to G54-P57 ablation in the CAP1/Prss8 protein, indicating that mouse *fr* and the rat fr^{CR} mutations may indeed be orthologues [16], as already suggested by previous studies [20]. Therefore, the V170D missense and G54-P57 deletion mutations in the *CAP1/Prss8* gene have been proposed as the molecular bases for the *fr* mouse and fr^{CR} rat variants, respectively.

Aiming to investigate whether these genetic data could be supported by molecular and functional evidences, we analyzed the consequences of those mutations, and performed *in silico*, *in vitro* and *in vivo* experiments. V170D and G54-P57 deletion mutations changed CAP1/Prss8 protein structure and reduced ENaC activation in the *Xenopus laevis* oocyte cell system. Inheritance, histological and functional studies of fr/fr, fr/Δ mice and fr^{CR}/fr^{CR} rats in comparison with littermate control groups, unveiled very similar features among these

variants, defined by reduced embryonic viability, skin abnormalities, and decreased ENaC activity in the distal colon. Therefore, we could demonstrate, at the molecular and functional level, that the *fr* and fr^{CR} phenotypes are caused by V170D and G54-P57 deletion mutations in the *CAP1/Prss8* gene. Finally, *fr* and fr^{CR} animals emerged as suitable models for CAP1/Prss8 reduced function in the whole organism.

MATHERIALS AND METHODS

Homology modeling, *in silico* alanine scanning and amino acid alignment

Mouse CAP1/Prss8 45-290 sequence fragment obtained from the CAP1/Prss8 entry Q9ESD1 at the UniProt knowledgebase [21] was a target sequence for homology modeling of murine CAP1/Prss8 structure. As a template the crystal structure of human homologous protein available in the protein structures database under the 3DFJ code was used [22]. The alignment between the two sequences was built using the Modeller 9v5 program [23]. A very high, 80% sequence identity between the target and the template sequence in the calculated alignment implies a good reliability of the final model. The standard modeling procedure using spatial restraints derived from the alignment was performed with Modeller 9v5. The 100 models were constructed and their ANOLEA scores [24] were calculated. The model with the best overall ANOLEA score was chosen for further studies. The quality of the model was checked with the PROCHECK software. Noteworthy, no residues were appearing in the disallowed regions of Ramachandran plot and 91.1% of residues appeared in the most favored regions of the plot indicating the good quality of the structure. The FoldX program [25] was employed to perform a computational alanine scan by mutating selected residues to an alanine and estimating the change in the protein stability. Amino acid alignment was performed by using the clustalw2 program (http://www.ebi.ac.uk/Tools/msa/clustalw2/).

Construct preparation, *Xenopus* oocyte injections, electrophysiological measurements and HEK-293 cells transfections

The T to A transversion that results in a valine to aspartate substitution at residue 170, and the GGTCAGTGGCCC deletion that results in G54-P57 ablation in the transcribed protein, were each inserted into the mouse *CAP1/Prss8* coding sequence (Genbank g.i. 19111159) and introduced in the pSDeasy expression vector, a modified pSD5 vector [26], for in vitro transcription. SP6 RNA polymerase (Promega) was used for cRNA synthesis.

Expression studies performed in *Xenopus laevis* oocytes (Noerdhoek, South Africa) in stage V/VI, were described previously [27]. A total of 0.25 ng of each cRNA encoding the three rat ENaC subunits in the presence or absence of 2 ng of wild-type or mutant CAP1/Prss8 cRNA in a total volume of 50 nl was injected into oocytes. Oocytes were incubated in modified Barth saline solution. Twenty-four hours after cRNA injection, electrophysiologic measurements were performed using the two-electrode voltage clamp technique. The amiloride-sensitive current was measured in the presence of 120 mM Na^+ in frog Ringer with and without 5 μM amiloride and without 20mg/ml of trypsin at a holding potential of -80mV.

Wild-type and mutant mouse *CAP1/Prss8* coding sequences were inserted in the pRK5 expression vector for HEK-293 cells transfection. HEK-293 were cultured in Dulbecco's modified Eagle's medium (DMEM) supplemented with 10% fetal calf serum and gentamycin (100 μg/ml) and transfected at 50–60% confluence in 100-mm dishes using the calcium-phosphate method. After transfection, cells were grown for 48 h in DMEM supplemented with 10% fetal calf serum before harvesting. The total amount of transfected DNA was 12 μg/100-mm dish.

Western blot and pulse-chase experiments

Xenopus oocytes were homogenized in Triton X-100 1%, Tris-HCl 20 mM, pH 7.6 and NaCl 100 mM. Lysates were centrifuged (13,000 *g* for 10 min at 4 °C). HEK-293 cells were lysed using 1 ml of lysis buffer per dish of 1% Triton Buffer (20mM Tris-HCl pH7.4, 150mM NaCl, 1% Triton X-100, 100mM leupeptin, pepstasin and aprotinin, 10mM PMSF). HEK-293 cells lysates were incubated 1 h at 4 °C on a rotating wheel. The solubilized material was centrifuged at 10,000 x g for 30 min at 4 °C and the supernatants were collected. Animal tissues were lysed in 1 ml of RIPA buffer (50mM Tris-HCl pH7.2, 150mM NaCl, 1% NP-40, 0.1% SDS, 0.5% Na-deoxycholate, 100mM leupeptin, pepstasin and aprotinin, 10mM PMSF). Lysates were centrifuged (13,000 *g* for 15 min at 4 °C) and the supernatants were

collected. For SDS-PAGE, samples were loaded and separated on a 10% polyacrylamide gel. Western blot analysis was performed using rabbit anti-mouse antibodies to CAP1/Prss8 [28]. Signals were revealed using anti-rabbit immunoglobulin G from goat (1:10,000) as secondary antibody and the SuperSignal West Dura detection system (Pierce).

To study CAP1/Prss8 protein expression, cRNA-injected oocytes were incubated in modified Barth's solution (MBS) containing 0.7-1 mCi/ml [35S]methionine for 6 h and subjected to 4- and 16-h chase periods in MBS containing 10 mM unlabeled methionine. After the pulse-chase periods, protein extracts were prepared and subjected to non-denaturing immune-precipitations [29]. After overnight incubation at 4°C with CAP1/Prss8 antibody, the immune-complexes were recovered on protein A Sepharose beads (GE Healthcare) and washed several times with MBS containing unlabeled methionine. Immunoprecipitates were resolved by SDS-PAGE (10% polyacrylamide) gels.

Isolation of rat alveolar epithelial cells

The procedure of rat alveolar epithelial cell (AEC) isolation accorded with legislation currently in force in France and Switzerland, and animal welfare guidelines (Ministère Français de la Pêche et de l'Agriculture, agreement # 5669). Alveolar epithelial cells were isolated from adult wild type, heterozygous and homozygous mutant rats by elastase digestion of lung tissue followed by sequential filtration and differential adherence on bacteriological dishes as previously described [28]. Cell purity was >80%, and cell viability > 95%.

Preparation of alveolar epithelial cell protein extracts and Western blotting procedure

Freshly isolated rat AEC were resuspended in 30 µl of ice-cold lysis buffer containing 150 mM NaCl, 50 mM Tris-HCl (pH 7.6), 1% Triton X-100, 0.1% SDS, and protease inhibitors, and kept on ice for 1h. Cell lysates were then centrifuged (12,000 rpm, 15 min) at 4°C, and samples of the supernatants were immediately frozen before use. For Western blotting, samples of protein extracts (40 µg protein) in one volume of sample buffer (containing 13.8%

sucrose, 9.6% SDS, 4.2% beta-mercaptoethanol, and 0.0126% bromophenol blue in H_2O) were resolved through 10% acrylamide gels, electroblotted, electrically transferred to PVDF membranes, and subsequently probed for CAP1 protein detection. The goat anti-rabbit IgG secondary antibody (Santa Cruz Biotechnology) was used at dilution 1:3,000, and the signal was developed with the Western Bloting Luminol Reagent (Santa Cruz Biotechnology).

Animal genotyping and stool assay

The genotype of *fr* mouse and fr^{CR} rat animal models (kindly provided by Dr. Thomas R. King; Biomolecular Sciences, Central Connecticut State University, 1615 Stanley Street, New Britain, CT 06053, USA) was assessed as formerly described [16]. We previously reported the generation and genotyping of the engineered null allele (*Δ*) of *CAP1/Prss8* [19]. Experimental procedures and animal maintenance followed federal guidelines and were approved by local authorities. All animals were housed in a temperature and humidity controlled room with an automatic 12 h light/dark cycle, and had free access to food and tap water.

Faecal hydration was assessed as following: freshly evacuated stools were collected in the morning, and weighted prior to and after at least 2 hours of dehydration performed by using the SpeedVac. Values are expressed as mean of the difference in weight ± s.e.m.

RNA extraction and quantitative RT-PCR.

Cells and organs were homogenized using Tissue Lyser (Qiagen) and RNA was extracted with the Qiagen RNeasy Mini kit following the manufacturer's instructions. 1 μg of RNA was reverse-transcribed using M-MLV Reverse Transcriptase RNase H Minus Point Mutant (Promega). Real-time PCR was performed by TaqMan PCR using Applied Biosystems 7500. Each measurement was taken in duplicate. Quantification of fluorescence was normalized to beta-actin. Primer and probe sequences were published previously [1].

Immunofluorescence and histology

Cells and organs were embedded into paraffin. Slides were incubated in xylene for at least four hours and rinsed with decreasing concentrations of ethanol. Antigen retrieval was performed for 10 min in TEG buffer. Slides were washed in 50 mM NH4Cl in PBS for 30 min and blocked by 1% BSA, 0.2% gelatine, 0.05% Saponin in PBS at room temperature for 10 min, three times. Primary antibody was diluted in 0.1% BSA, 0.3% Triton X-100 in PBS, overnight at 4 °C. Affinity-purified CAP1/Prss8 rabbit anti-mouse antiserum [28] was diluted 1:200. Slides were rinsed three times for 10 min in PBS containing 0.1% BSA, 0.2% gelatine and 0.05% saponin at room temperature and the secondary antibody (Alexa Fluor 488, diluted 1:5,000) was diluted in 0.1% BSA, 0.3% Triton X-100 in PBS. Staining was visualized using an LSM confocal microscope (LSM 510 Meta, Carl Zeiss MicroImaging Inc.).

Hematoxylin and eosin colorations were performed as following: the paraffine was removed and the slides re-hydrated 2x in xylol for 5', 2x in 100% ethanol for 1 min, in 95% ethanol for 1 min and finally with tap water. The coloration was performed as follows: Glychemalun solution (Hematein 0.013 M, Gurr #34036; potassium alum 0.3133 M, Merk #1047; 30% glycerol; 1% acetic acid Merk #1.00063) for 4 min, tap water, 1% acid alcohol for 3 sec, tap water, water for 15 sec plus a few drops of NH_3, tap water, 0.2% erythrosine solution (Erythrosin 0.0023 M, Merk #15936; Formol 0.1%, Merk #4003) for 30 sec and finally tap water. Slides were then de-hydrated by following steps from 70% ethanol to xylol and mounted (Eukitt). Pictures were taken using an Axion HRC (Carl Zeiss MicroImaging Inc.).

Measurement of trans epithelial water loss (TEWL) and rectal trans epithelial potential difference (PD)

The rate of TEWL from the ventral skin of pre-shaved, anaesthetized animals was measured using a Tewameter TM210 (Courage and Khazaka). The mean ± s.e.m. is shown.

Rectal PD and amiloride-sensitive rectal PD were measured in the morning (10 a.m –12 p.m.) and in the afternoon (4 p.m. – 6p.m.) of two different days of the same week. Animals were anaesthetized with an intra-peritoneal injection of Ketalar (Park-Davis, Baar, Switzerland; 75 mg/g bodyweight) and Rompun (Bayer, Leverkusen, Germany; 2.3 mg/g bodyweight) and placed on a heated table. A winged needle filled with isotonic saline was placed in the subcutaneous tissue of the back. A double-barreled pipette was prepared from borosilicate glass capillaries (1.0 mm OD/0.5 mm ID; Hilgerberg, Malsfeld, Germany) and pulled to an approximate 0.2 mm tip diameter. The first barrel was filled with isotonic saline buffered with 10 mM Na^+-HEPES (pH 7.2) and the second barrel was filled with the same solution containing 25 mM amiloride. The tip of the double-barreled pipette was placed in the rectum approximately 3-5 mm from the skin margin. The electrical PD was measured between the first barrel and the subcutaneous needle, both connected to Ag/AgCl electrodes by means of plastic tubes filled with 3 mM KCl in 2% agar. The rectal PD was monitored continuously by a VCC600 electrometer (Physiologic Instruments, San Diego, CA, USA) connected to a chart recorder. After stabilization of the rectal PD (approximately 1 min), 0.05 ml saline solution was injected through the first barrel as a control manoeuvre and the PD was recorded for another 30 sec period. A similar volume of saline solution containing 25 mM amiloride was injected through the second barrel of the pipette and the PD was recorded for another 1 min. The amiloride-sensitive PD was calculated as the difference between the PD recorded before and after the addition of amiloride.

RESULTS

Reduced ENaC activation of V170D and G54-P57 CAP1/Prss8 deletion mutant proteins.

Taking the advantage of the *in silico* protein modeling technique, we built the homology model of the mouse CAP1/Prss8 (Fig. 1A), using as template the crystal structure-based homology model of human CAP1/Prss8 [30]. V170 belongs to one of the beta strands in the inside of the protein, and is located in a hydrophobic environment. V170 makes hydrophobic contacts with the methyl groups of V256 and L191. The alanine scanning for V170 resulted in 2.4 Kcal loss of energy upon mutation to Ala. G54-P57 residues (Gly-Gln-Trp-Pro) in CAP1/Prss8 are found on the external surface of the molecule and therefore solvent-exposed. This fragment, which is deleted in the fr^{CR}/fr^{CR} mutant rats, contains the structurally important Trp56 leading to 4.5 Kcal loss in stability when mutated to Ala. Multiple sequence alignments illustrated that the mutated residues are conserved among different species (Fig. 1B).

To investigate the consequences of the V170D and G54-P57 deletion mutations on *CAP1/Prss8* expression and function, we introduced V170D and G54-P57 deletion mutations in the mouse *CAP1/Prss8*, inserted the cDNA sequences in the pSDeasy expression vector for *in vitro* transcription [26], and co-injected CAP1/Prss8 and ENaC cRNA in the *Xenopus* oocytes. CAP1/Prss8 cRNA stability was estimated by real-time PCR, and no remarkable difference in the level of each V170D and G54-P57 deletion mutant versus wild-type *CAP1/Prss8* was observed (data not shown). CAP1/Prss8 immuno-staining was detected at the plasma membrane in oocytes that were injected with wild-type CAP1/Prss8, and equal results were obtained with V170D and G54-P57 deletion CAP1/Prss8 mutants (Fig. 2A). Western blot analysis against CAP1/Prss8 evidenced the presence of two bands, of 37 and 40 KDa, that might correspond to two different glycosylation states of the protein, and showed that the two mutant proteins can be translated as well as the wild-type (Fig. 2B).

Glycosylation of CAP1/Prss8 was assessed by treatment of oocyte extracts with the de-glycosylating enzyme PNGase F, that revealed the presence of a non-glycosylated (n) native form upon de-glycosylation treatment. Thus, the two bands of 37 and 40 KDa, most likely correspond to the core-glycosylated form (c), which is typical of newly synthetized proteins, and the fully-glycosylated form (f) characteristic of mature proteins, respectively (Fig. 2C). Analogous results were obtained in transfected HEK-293 cells (Fig. 2D).

To get further insight not only into the production but also into the degradation of wild-type and mutant proteins, we performed pulse-chase experiments by pulsing radioactively the oocytes during 6 hours (P) and chasing them during 4 (C1) and 16 (C2) hours in unlabeled media. Wild-type CAP1/Prss8 protein production was evident after 6 hours of pulse, and protein degradation was observed already following the first chase period. Similar results were obtained for the two mutant proteins. However, CAP1/Prss8 V170D and G54-P57 deletion mutants showed different glycosylation states in comparison with the wild-type CAP1/Prss8, evidencing an increased fully-glycosylated state of the G54-P57 deletion mutant versus an increased core-glycosylated state of the V170D mutant (Fig. 2E).

Co-expression of wild-type CAP1/Prss8 with ENaC leads to a significant increase in the amiloride-sensitive sodium current in the *Xenopus* oocyte cell system [31], hence ENaC current is considered an appropriate parameter to monitor CAP1/Prss8 activity. Trypsin can activate near-silent ENaC channels by dramatically increasing its open probability, indicating maximal ENaC activity of the cells [32]. Co-injection of wild-type CAP1/Prss8 and ENaC revealed a 3.7-fold significant increase in the amiloride-sensitive sodium current relative to trypsin, compared to oocytes that were injected with ENaC alone. In contrast, when either CAP1/Prss8 V170D or G54-P57 deletion mutant was co-expressed with ENaC, the ability of CAP1/Prss8 to increase ENaC-mediated currents was significantly reduced, leading to a 2.8 and 2.1-fold increase relative to trypsin, respectively (Fig. 2F).

Reduced viability and similar hair phenotype in *fr* mouse and *fr*^{CR} rat models.

To study the consequences of CAP1/Prss8 V170D and G54-P57 deletion mutations and to investigate whether they might be responsible of the phenotypes observed in the *fr* mouse and *fr*^{CR} rat models, we performed inheritance, histopathological, molecular and functional analyses of *fr/fr*, *fr/Δ* and *fr*^{CR}/*fr*^{CR} versus control littermates.

Each *fr/fr* and *fr/Δ* mouse variants presented reduced prenatal viability, deriving from crosses *fr*/+ x *fr/Δ*, yielding only about 16% *fr/fr* and 13% *fr/Δ* mutant offspring respectively, rather than the expected 25%. *fr*^{CR}/+ x *fr*^{CR}/+ rat crosses generated 10% *fr*^{CR}/*fr*^{CR} mutants instead of the expected 25%. 83% of the *fr*^{CR}/*fr*^{CR} rats resulted in males (Table I).

fr/fr, *fr/Δ* and *fr*^{CR}/*fr*^{CR} animals were distinguishable from their siblings as soon as the hair started to grow. In comparison to wild-type controls, *fr/fr* mice manifested curly whiskers and a wavy coat. The phenotype of *fr/Δ* animals was more severe, showing curly whiskers accompanied by less and shorter hair. *fr*^{CR}/*fr*^{CR} rats were almost completely bald. These data are in accordance with previous observations [16,20].

No histopathological aberrations were observed in lung, kidney and distal colon. In contrast, *fr/fr*, *fr/Δ* mice and *fr*^{CR}/*fr*^{CR} rats presented hair bulbs deeply positioned in the lower dermis. In addition, *fr*^{CR}/*fr*^{CR} skin exhibited hyperplasic epidermis and hyperkeratosis, as well as swelled and more abundant sebaceous glands. Beside these structural and morphological defects, no signs of inflammation, such as cellular infiltrations, were detectable in *fr/fr*, *fr/Δ* and *fr*^{CR}/*fr*^{CR} mutant skin (Fig. 3).

Aiming to investigate CAP1/Prss8 expression at the transcriptional level, we performed quantitative real time PCR analyses on skin, lung, kidney and colon extracts of *fr/fr*, *fr/Δ* mutant mice and control littermates. For all analyzed organs, mice carrying *Δ*/+ alleles, presented a significant (50%) reduction in the expression of *CAP1/Prss8* when compared to wild-type animals, as it might be predicted from the absence of one *CAP1/Prss8* allele.

Decreased *CAP1/Prss8* expression was detected also in *fr/Δ* heterozygous, but it was significant only in the kidney. CAP1/Prss8 mRNA levels in *fr/fr* mutants did not differ from that of wild-type animals (Fig. 4A). Analogous analyses in the skin of fr^{CR}/fr^{CR} mutant rats in comparison to wild-types revealed a significant two-fold increase in the mRNA expression of *CAP1/Prss8*. In contrast, *CAP1/Prss8* was significantly reduced in the distal colon (Fig. 4B), while no significant changes were observed among the different genotypes in lung and kidney.

Finally, we performed western blot analyses using CAP1/Prss8 antibody on kidney, lung and alveolar epithelial cell extracts from *fr* mice and fr^{CR} rats, respectively. CAP1/Prss8 detection in *fr/Δ* and *fr/fr* mice evidenced a preferential core-glycosylated state of the mutant protein in comparison with the wild-type (Fig 4C). CAP1/Prss8 detection in fr^{CR}/fr^{CR} rats evidenced a preferential fully-glycosylated state compared to controls (Fig 4D). These data are entirely in accordance with the results obtained *in vitro*.

Reduced body weight and dehydration defects in fr^{CR}/fr^{CR} rats.

fr/fr and *fr/Δ* mouse mutants did not present differences in body weight in comparison with controls (Fig. 5A). fr^{CR}/fr^{CR} rats appeared smaller and exhibited a significantly lower body weight compared to wild-type and heterozygous littermates (Fig. 5B). To investigate whether the macroscopical and histological defects in *fr/fr*, *fr/Δ* and fr^{CR}/fr^{CR} mutants were accompanied by functional abnormalities of the skin, and to explore the ability of this organ to protect the body against excessive dehydration, we measured the trans epidermal water loss (TEWL). *fr/fr* and *fr/Δ* mouse mutants did not differ from controls with respect to the TEWL (Fig. 5C). In contrast, fr^{CR}/fr^{CR} rats exhibited a significant increase in the TEWL, suggesting that the skin barrier is compromised in these animals (Fig. 5D). Moreover, fr^{CR}/fr^{CR} rats presented diarrhea accompanied by increased stool hydration (Fig. 5E and F).

Significantly decreased ENaC activity in the distal colon of *fr/fr*, *fr/Δ* and fr^{CR}/fr^{CR} animals

CAP1/Prss8 can increase ENaC-mediated sodium currents [6,31]. To query the effect of *CAP1/Prss8* V170D and G54-P57 deletion mutations on ENaC activity *in vivo*, the amiloride-sensitive rectal potential difference was measured in the distal colon of both, *fr* mouse and fr^{CR} rat animal models. Since amiloride is a specific and potent inhibitor of ENaC [33], the amiloride-sensitive potential difference is an indirect indicator of ENaC function. Rectal potential difference in rodents follows circadian variation, reflecting differential metabolic activity of the animals during the day [34]. We therefore performed *in vivo* measurements both in the morning and in the afternoon of two different days. *Δ*/+ and *fr*/+ heterozygotes did not manifest differences compared to the wild-types. *fr/fr* and *fr/Δ* mice revealed a significant decrease in the amiloride-sensitive potential difference, reflecting a significantly reduced ENaC activity in the distal colon (Fig. 6A). As *fr/fr* and *fr/Δ* mice, fr^{CR}/fr^{CR} rats demonstrated a significant less negative potential difference. Surprisingly, fr^{CR}/+ heterozygous rats showed reduced potential difference only in the morning, while in the afternoon the values were not different from wild-types (Fig. 6B).

DISCUSSION

In this manuscript we study whether the spontaneous V170D and G54-P57 deletion mutations within the *CAP1/Prss8* gene of 'frizzy' mice (*fr*) and 'hairless' rats (fr^{CR}) respectively, may cause their skin phenotypes and have additional consequences on the homeostasis of various organs where CAP1/Prss8 is expressed.

In silico experiments indicated that the mutation V170D may alter CAP1/Prss8 protein structure because of unfavorable interactions of hydrophobic side-chains with polar Asp, and, most likely, the change of V170 to Asp would lead a more severe modification of the three-dimensional configuration than the 2.4 Kcal loss of energy upon mutation to Ala. G54-P57 residues in CAP1/Prss8 resulted solvent exposed, and their deletion could have a considerable impact on folding and architecture of the protein. These alterations of the protein structure may modify the interaction of CAP1/Prss8 with its effectors. We and other researchers have demonstrated that CAP1/Prss8 can increase the activity of the epithelial sodium channel ENaC in various expression systems [8,31,35], therefore CAP1/Prss8 activity can be evaluated by measuring ENaC currents. When we injected CAP1/Prss8 V170D and G54-P57 deletion mutants in the *Xenopus* oocytes, we observed that these mutations do not prevent the expression of the protein at the plasma membrane and their capability to activate the channel when co-expressed. However, the ability of CAP1/Prss8 V170D and G54-P57 deletion mutants to stimulate ENaC appeared significantly decreased. Western blot analyses and pulse-chase experiments revealed a differential glycosylation state of the two mutant proteins in comparison with the wild-type CAP1/Prss8, evidencing a preferential core-glycosylated state of the V170D mutant versus a preferential fully-glycosylated state of the G54-P57 deletion mutant, indicating an increased retention of the V170D mutant in the endoplasmic reticulum (ER) and enhanced intracellular transport of the G54-P57 deletion mutant. In addition to the changes in the glycosylation state, pulse-chase experiments demonstrated that the degradation

and thus the stability of the mutant proteins do not change in comparison with the wild-type. However, what it does differ is the amount of energy lost upon mutation of V170 and W56 to Ala, as indicated by *in silico* alanine scanning. This loss of energy might modify the three-dimensional conformation of the mutant proteins, that may be responsible of a differential glycosylation state, and eventually reduce their activity.

To determine the role of *CAP1/Prss8* in the different tissues, we previously deleted the mouse *CAP1/Prss8* gene locus, located on chromosome 7, in a temporally and/or tissue-specific manner [19], and revealed crucial roles for this serine protease at least in the skin and in the lung [7,6,1]. *fr/fr*, *fr/Δ* mice and fr^{CR}/fr^{CR} rats displayed a significant reduction in the embryonic viability compared to the expected Mendelian inheritance, coinciding with the prenatal lethality of the *CAP1/Prss8* knock-out mice, and strongly indicating a pleiotropic role of CAP1/Prss8 in embryonic development. Very interestingly, similar histopathological alterations occurred in the skin of *fr/fr*, *fr/Δ* and fr^{CR}/fr^{CR} animals, denoting that both mouse and rat skin structure is sensitive to *CAP1/Prss8* mutations and altered function. Skin anomalies in 'frizzy' and 'hairless' animals did not appear to be accompanied by inflammation, thus these defects might originate during embryonic development and hair morphogenesis. Interestingly, fr^{CR}/fr^{CR} rats exhibited, in addition to alopecia and hyperkeratosis, an increase in the size and number of sebaceous glands. Sebum is a mixture of lipids [36] that coat the fur as a hydrophobic protection against dehydration and for heat insulation [37], and fr^{CR}/fr^{CR} animals may compensate their excess in loss of water through the skin by increasing the production of sebum.

The *fr* mutation first appeared in 1949 at the Jackson Laboratory, and was identified in 1951 by Falconer and Snell on a mixed genetic background that included the genetically linked recessive visible markers pink-eyed dilution (p), chinchilla (Tyrch), and shaker-1 (Myo7a) [38]. We consider unlikely that those or other additional mutations in *fr/fr* animals could contribute

to the phenotype, since the same phenotype is maintained or even enhanced in the *fr/Δ* animals, and absent in the heterozygotes. In contrast, we can not exclude the implications of additional recessive mutations on the phenotype of fr^{CR}/fr^{CR} rats, and a complementation test could solve this issue, but so far CAP1/Prss8 knock-out alleles in rats are not available. Additional mutations in fr^{CR}/fr^{CR} animals could be responsible of the baldness and of the permeability defects observed in the skin and in the intestine of mutant rats, but not in *fr/fr* and *fr/Δ* mice. Alternatively, baldness and permeability defects in fr^{CR}/fr^{CR} rats could be the result of more severe consequences generated by the *CAP1/Prss8* G54-P57 deletion mutation compared to the *CAP1/Prss8* V170D mutation, or might be species-dependent.

Although decreased in the distal colon, *CAP1/Prss8* transcription levels increased in the skin of fr^{CR}/fr^{CR} rats, and a tendency for CAP1/Prss8 mRNA levels to augment could be noticed also in *fr/Δ* mice, not only in the skin but also in colon and lung. These data show a different transcriptional regulation of mutated CAP1/Prss8 in different organs, and a transcriptional up-regulation of mutated *CAP1/Prss8* in *fr/Δ* mice, that might be due to compensatory effects.

Dehydration defects, either caused by skin or intestine anomalies, are often accompanied by body weight loss [39,40]. Both skin-specific *CAP1/Prss8* knock-out and *CAP1/Prss8* overexpressing mice presented increased skin dehydration accompanied by loss in body weight [7,1] and the tight junction functionality was defective in the skin-specific *CAP1/Prss8* knock-outs [7]. Similarly, fr^{CR}/fr^{CR} rats showed significant reduction in body weight and manifested increased loss of water through the skin and intestine, evidencing epidermal permeability barrier defects that might be due to an effect of mutant *CAP1/Prss8* on tight junctions and/or on sodium and therefore water reabsorption. ENaC activity resulted dramatically reduced in the distal colon of mutant mice and rats, and this decrease resulted of the same extent as that observed in intestine-specific *CAP1/Prss8* knock-out mice (Sumedha Malsure et al., manuscript in preparation, Edith Hummler laboratory). These data indicate that

fr/fr, *fr/Δ* animals exhibit the same reduction in the basal activity of ENaC as that of *CAP1/Prss8* loss-of-function mutants.

The three subunits of ENaC are expressed by surface epithelial cells of the distal colon [41] and several serine proteases that activate ENaC *in vitro* are also expressed in the gastrointestinal tract, with a tissue distribution broader than ENaC. CAP1/Prss8 is present in stomach and colon in rats, and in stomach, small intestine and distal colon in mice [35,31]. The activity of ENaC depends on more than one serine protease, and we have previously shown that the serine protease CAP3/matriptase is able to increase 6 to 10-fold ENaC currents [31]. It is noteworthy that both skin-specific deletion of *CAP1/Prss8* and complete abrogation of *CAP3/matriptase* in mice caused leaky skin barrier [42,7], and that intestine-specific deletion of *CAP3/matriptase* provoked colon enlargement, persistent diarrhoea and increased intestinal paracellular permeability [43]. Moreover, CAP1/Prss8 and CAP3/matriptase are constitutively co-localized in most epithelia [44] and have been proposed to be involved in the same proteolytic cascade [11,45]. Thus, it is presumable that CAP1/Prss8 and CAP3/Tmprss14 cooperate to maintain the homeostasis of different organs.

In conclusion, the present study shows that both *fr* mouse and fr^{CR} rat models share similar features, like reduced embryonic viability, abnormal allocation of hair follicles in the dermis, and reduced amiloride-sensitive sodium current in the distal colon. All together these data support that *fr* and fr^{CR} are mutant alleles of the *CAP1/Prss8* gene. *fr* and fr^{CR} therefore appear as suitable models for *CAP1/Prss8* decreased function in the whole organism, and the consequences of mutated *CAP1/Prss8* on its effectors and related pathways will be the object of further research.

ACKNOWLEDGEMENTS

We thank Dr. Thomas R. King (New Britain, CT 06053, USA) for kindly providing the *fr* and fr^{CR} animal models, Professor Kaethi Geering and Professor Bernard C. Rossier for helpful suggestions and critical reading of the manuscript, and all the members of the Hummler lab for discussions. We also thank Dr. Dominique Marchant for technical assistance with the Western blot on isolated alveolar epithelial cell extracts. We are grateful to the Mouse Pathology platform and the Cellular Imaging Facility platform, University of Lausanne. This work was supported by the Swiss National Science Foundation (Grant 3100A0-102125/1 to E. Hummler), the Swiss National Centre of Competence in Research (NCCR) Kidney Control of Homeostasis (Kidney.CH), and the Leducq Fondation.

Figure legends

Figure 1. A: Homology model of the mouse CAP1/Prss8 tertiary protein structure constructed on the crystal structure-based homology model of the human CAP1/Prss8. Val170 residue, mutated into Asp in the *fr* mouse variant (upper panels, entire and zoomed view) and the Gly54-Gln-Trp-Pro57 fragment, deleted in the fr^{CR} rat variant (lower panels, entire and zoomed view) are highlighted in red. The residues of the serine protease active site, Asp134, His85 and Ser238 are represented in yellow. The hydrophobic environment of Val170 consists of Ile45, Leu191 and Val256 shown in dark blue, as well as Asp237 in cyan. Gly54-Pro57 interact with adjacent residues: Trp triad formed by Trp 56 (red) and Trp58 and Trp250 (in dark green), Gln190 (in cyan) side chain forming hydrogen bond with Trp56 and hydrogen bond formed by Gln55 and Lys52 backbone. **B:** Amino acid alignment of the full length protein of mouse (gi: 19111160), rat (gi: 20301968) and human (gi: 4506153) CAP1/Prss8 performed using the ClustalW2 multiple sequence alignment program (http://www.ebi.ac.uk/Tools/msa/clustalw2/ Date of accession to the website: 17 August 2011). Mouse and rat share 92% of CAP1/Prss8 sequence identity, mouse and human 77%, and rat and human 75%. The amino acids of the catalytic triad (His, Asp, Ser) are indicated by arrows. The four residues deleted in the fr^{CR} rat (Gly, Gln, Trp, Pro) and the Val170 substituted with Asp in the *fr* mouse variants are indicated in red, and result conserved among these species. Stars indicate identical amino acid residues, double dots and dots indicate amino acids with similar and less similar side chain proprieties, respectively.

Figure 2. A: CAP1/Prss8 immunofluorescence (green) performed in *Xenopus* oocytes injected with ENaC and CAP1/Prss8 wild-type, V170D and G54-P57 deletion mutant cRNA. BF: bright field. **B:** Oocytes were injected as indicated and Western blot analyses were

performed on cell lysates using CAP1/Prss8 and beta-actin antibodies. Two representative experiments (exp. 1 and exp. 2) are shown and quantification relative to beta-actin was performed on a total of four independent experiments each consisting of at least five oocytes injected per condition. **C:** Oocytes were injected as in B and protein extracts were treated (+) or not (-) with PNGase F in order to de-glycosylate the proteins and then subjected to Western blot analysis using CAP1/Prss8 antibody. f: fully-glycosylated, c:core-glycosylated, n: non-glycosylated. **D:** HEK-293 cells were transfected as indicated and protein extracts were treated (+) or not (-) with PNGase F in order to de-glycosylate the proteins and then subjected to Western blot analysis using CAP1/Prss8 antibody. f: fully-glycosylated, c:core-glycosylated, n: non- glycosylated. This figure is representative of three independent experiments. **E:** Oocytes were injected as indicated and subjected to 6-h pulse (P), 4- (C1) and 16-h (C2) chase periods. After the pulse-chase periods, protein extracts were prepared and subjected to non-denaturing immune-precipitations using CAP1/Prss8 antibody. Two experiments (exp. 1 and exp. 2) are shown and are representative of three independent experiments each consisting of fifteen oocytes injected per condition. f: fully-glycosylated, c:core-glycosilated. **F:** Amiloride-sensitive sodium currents from four independent experiments pulled together each consisting of at least five oocytes measured per condition prior to and after trypsin perfusion. The currents measured before the perfusion of the oocytes with trypsin were normalized to currents measured after trypsin perfusion. ***p<0.001

Figure 3. Hematoxylin and eosin staining of skin, colon, lung and intestine in *fr* mouse (+/+, *fr*/+, Δ/+, *fr*/Δ, *fr*/*fr*) and fr^{CR} rat (+/+, fr^{CR}/+, fr^{CR}/fr^{CR}) variants, performed in young-adult animals. Scale bar indicates 20 μm.

Figure 4. A: *CAP1/Prss8* mRNA levels, relative to beta-actin, investigated by quantitative real time PCR, in lung, skin, colon and kidney of *fr* mice (+/+ n=10; *fr*/+ n=6; Δ/+ n=8; *fr*/Δ n=4; *fr/fr* n=9 number of analyzed animals). **B:** *CAP1/Prss8* mRNA levels, relative to beta-actin, investigated by quantitative real time PCR, in lung, skin, colon and kidney of fr^{CR} rats (+/+ n=4; fr^{CR}/+ n=4; fr^{CR}/fr^{CR} n=4 number of analyzed animals). *p<0.05, **p<0.01, ***p<0.001. **C:** Western blot analysis performed on kidney extracts from *fr* mice using CAP1/Prss8 antibody. f: fully-glycosylated, c:core-glycosylated, a: aspecific band. Analogous results were obtained from lung extracts. Three animals per genotype were analyzed. **D:** Western blot analysis using CAP1/Prss8 antibody performed on lung alveolar epithelial cells isolated from fr^{CR} rats. f: fully-glycosylated, c:core-glycosylated. Two animals per genotype were analyzed.

Figure 5. A: Body weight measurements expressed in grams (gr.) of *fr* mice (+/+ n=12; *fr*/+ n=15; Δ/+ n=23; *fr*/Δ n=13; *fr/fr* n=22 number of analyzed animals), performed in young-adult animals. n.s.= non significant. **B:** Body weight measurements expressed in grams (gr.) of fr^{CR} rats (+/+ n=8; fr^{CR}/+ n=8; fr^{CR}/fr^{CR} n=10; ***p<0.001, male rats only), performed in young-adult animals. Same results were obtained for female rats (+/+ 283±6.2 n=6; fr^{CR}/+ 296±6.6 n=7; fr^{CR}/fr^{CR} 259±12.1 n=4; p<0.05). **C:** Trans-epidermal water loss (TEWL) measurements of *fr* mice (+/+ n=10; *fr*/+ n=5; Δ/+ n=8; *fr*/Δ n=5; *fr/fr* n=9) expressed in grams on square meters per hour (gr./[m^2h]). **D:** TEWL measurements of fr^{CR} rats (+/+ n=4; fr^{CR}/+ n=4; fr^{CR}/fr^{CR} n=4; *p<0.05) expressed in grams on square meters per hour (gr./[m^2h]). **E:** Representative pictures of the intestinal content of fr^{CR}/fr^{CR} and wild-type rats clearly show an increased liquid content in the stools of the fr^{CR}/fr^{CR} mutants. **F:** Faeces water content, assessed as difference between freshly collected and completely dehydrated stools (+/+ n=6; fr^{CR}/+ n=3; fr^{CR}/fr^{CR} n=7; *p<0.05).

Figure 6. A: Amiloride-sensitive rectal potential difference (PD), reflecting ENaC activity and expressed in mV, measured in the distal colon of *fr* mice (+/+, n=12; *fr*/+ n=12; Δ/+ n=13; *fr*/Δ n=10; *fr/fr* n=10). +/+ versus *fr/fr*, $p<0.05$. +/+ versus *fr*/Δ, $p<0.01$. **B:** Amiloride-sensitive rectal potential difference (PD), reflecting ENaC activity and expressed in mV, measured in the distal colon of fr^{CR} rats (+/+ n=4; fr^{CR}/+ n=4; fr^{CR}/fr^{CR} n=4). Measurements were performed both in the morning (A.M.) and in the afternoon (P.M.) of two different days (day 1 and day 2). +/+ versus fr^{CR}/fr^{CR}, $p<0.05$.

REFERENCES

1. Frateschi S, Camerer E, Crisante G, Rieser S, Membrez M, Charles RP, Beermann F, Stehle JC, Breiden B, Sandhoff K, Rotman S, Haftek M, Wilson A, Ryser S, Steinhoff M, Coughlin SR, Hummler E: PAR2 absence completely rescues inflammation and ichthyosis caused by altered CAP1/Prss8 expression in mouse skin, Nature communications 2011, 2:161
2. Puente XS, Sanchez LM, Overall CM, Lopez-Otin C: Human and mouse proteases: a comparative genomic approach, Nature reviews 2003, 4:544-558
3. Puente XS, Sanchez LM, Gutierrez-Fernandez A, Velasco G, Lopez-Otin C: A genomic view of the complexity of mammalian proteolytic systems, Biochemical Society transactions 2005, 33:331-334
4. Rawlings ND, Morton FR, Kok CY, Kong J, Barrett AJ: MEROPS: the peptidase database, Nucleic acids research 2008, 36:D320-325
5. Verghese GM, Tong ZY, Bhagwandin V, Caughey GH: Mouse prostasin gene structure, promoter analysis, and restricted expression in lung and kidney, American journal of respiratory cell and molecular biology 2004, 30:519-529
6. Planes C, Randrianarison NH, Charles RP, Frateschi S, Cluzeaud F, Vuagniaux G, Soler P, Clerici C, Rossier BC, Hummler E: ENaC-mediated alveolar fluid clearance and lung fluid balance depend on the channel-activating protease 1, EMBO molecular medicine 2009, 2:26-37
7. Leyvraz C, Charles RP, Rubera I, Guitard M, Rotman S, Breiden B, Sandhoff K, Hummler E: The epidermal barrier function is dependent on the serine protease CAP1/Prss8, The Journal of cell biology 2005, 170:487-496
8. Vallet V, Chraibi A, Gaeggeler HP, Horisberger JD, Rossier BC: An epithelial serine protease activates the amiloride-sensitive sodium channel, Nature 1997, 389:607-610
9. Vuagniaux G, Vallet V, Jaeger NF, Hummler E, Rossier BC: Synergistic activation of ENaC by three membrane-bound channel-activating serine proteases (mCAP1, mCAP2, and mCAP3) and serum- and glucocorticoid-regulated kinase (Sgk1) in Xenopus Oocytes, The Journal of general physiology 2002, 120:191-201
10. Narikiyo T, Kitamura K, Adachi M, Miyoshi T, Iwashita K, Shiraishi N, Nonoguchi H, Chen LM, Chai KX, Chao J, Tomita K: Regulation of prostasin by aldosterone in the kidney, The Journal of clinical investigation 2002, 109:401-408
11. Camerer E, Barker A, Duong DN, Ganesan R, Kataoka H, Cornelissen I, Darragh MR, Hussain A, Zheng YW, Srinivasan Y, Brown C, Xu SM, Regard JB, Lin CY, Craik CS, Kirchhofer D, Coughlin SR: Local protease signaling contributes to neural tube closure in the mouse embryo, Developmental cell 2010, 18:25-38
12. Satoru Takahashi SS, Shingo Inaguma, Yoshihisa Ikeda, Young-Man Cho, Norio Hayashi, Takahiro Inoue, Yoshiki Sugimura, Naoki Nishiyama, Tamio Fujita, Julie Chao, Toshikazu Ushijima, Tomoyuki Shirai: Down-regulated expression of prostasin in high-grade or hormone-refractory human prostate cancers, The Prostate 2003, 54:187-193
13. Chen LM, Chai KX: Prostasin serine protease inhibits breast cancer invasiveness and is transcriptionally regulated by promoter DNA methylation, International journal of cancer 2002, 97:323-329
14. Sakashita K, Mimori K, Tanaka F, Tahara K, Inoue H, Sawada T, Ohira M, Hirakawa K, Mori M: Clinical significance of low expression of Prostasin mRNA in human gastric cancer, Journal of surgical oncology 2008, 98:559-564
15. Mok SC, Chao J, Skates S, Wong K-k, Yiu GK, Muto MG, Berkowitz RS, Cramer DW: Prostasin, a Potential Serum Marker for Ovarian Cancer: Identification Through Microarray Technology, J Natl Cancer Inst 2001, 93:1458-1464

16. Spacek DV, Perez AF, Ferranti KM, Wu LK, Moy DM, Magnan DR, King TR: The mouse frizzy (fr) and rat 'hairless' (fr(CR)) mutations are natural variants of protease serine S1 family member 8 (Prss8), Experimental dermatology 2010,
17. Paul EL, Badal R, Thompson DS, Magnan DR, Soucy FM, Khan IM, Haughton RA, King TR: The mouse frizzy mutation (fr) maps between D7Csu5 and D7Mit165, Experimental dermatology 2008, 17:640-644
18. Panteleyev AA, Christiano AM: The Charles River "hairless" rat mutation is distinct from the hairless mouse alleles, Comparative medicine 2001, 51:49-55
19. Rubera I, Meier E, Vuagniaux G, Merillat AM, Beermann F, Rossier BC, Hummler E: A conditional allele at the mouse channel activating protease 1 (Prss8) gene locus, Genesis 2002, 32:173-176
20. Ahearn K, Akkouris G, Berry PR, Chrissluis RR, Crooks IM, Dull AK, Grable S, Jeruzal J, Lanza J, Lavoie C, Maloney RA, Pitruzzello M, Sharma R, Stoklasek TA, Tweeddale J, King TR: The Charles River "hairless" rat mutation maps to chromosome 1: allelic with fuzzy and a likely orthologue of mouse frizzy, The Journal of heredity 2002, 93:210-213
21. Hinz U: From protein sequences to 3D-structures and beyond: the example of the UniProt knowledgebase, Cellular and molecular life sciences : CMLS 2010, 67:1049-1064
22. Rickert KW, Kelley P, Byrne NJ, Diehl RE, Hall DL, Montalvo AM, Reid JC, Shipman JM, Thomas BW, Munshi SK, Darke PL, Su HP: Structure of human prostasin, a target for the regulation of hypertension, The Journal of biological chemistry 2008, 283:34864-34872
23. Eswar N, Webb B, Marti-Renom MA, Madhusudhan MS, Eramian D, Shen MY, Pieper U, Sali A: Comparative protein structure modeling using MODELLER, Curr Protoc Protein Sci 2007, Chapter 2:Unit 2 9
24. Melo F, Feytmans E: Assessing protein structures with a non-local atomic interaction energy, J Mol Biol 1998, 277:1141-1152
25. Schymkowitz J, Borg J, Stricher F, Nys R, Rousseau F, Serrano L: The FoldX web server: an online force field, Nucleic acids research 2005, 33:W382-388
26. Puoti A, May A, Rossier BC, Horisberger JD: Novel isoforms of the beta and gamma subunits of the Xenopus epithelial Na channel provide information about the amiloride binding site and extracellular sodium sensing, Proceedings of the National Academy of Sciences of the United States of America 1997, 94:5949-5954
27. Geering K, Theulaz I, Verrey F, Hauptle MT, Rossier BC: A role for the beta-subunit in the expression of functional Na+-K+-ATPase in Xenopus oocytes, The American journal of physiology 1989, 257:C851-858
28. Planes C, Leyvraz C, Uchida T, Angelova MA, Vuagniaux G, Hummler E, Matthay M, Clerici C, Rossier B: In vitro and in vivo regulation of transepithelial lung alveolar sodium transport by serine proteases, Am J Physiol Lung Cell Mol Physiol 2005, 288:L1099-1109
29. Geering K, Beggah A, Good P, Girardet S, Roy S, Schaer D, Jaunin P: Oligomerization and maturation of Na,K-ATPase: functional interaction of the cytoplasmic NH2 terminus of the beta subunit with the alpha subunit, The Journal of cell biology 1996, 133:1193-1204
30. Spraggon G, Hornsby M, Shipway A, Tully DC, Bursulaya B, Danahay H, Harris JL, Lesley SA: Active site conformational changes of prostasin provide a new mechanism of protease regulation by divalent cations, Protein Sci 2009, 18:1081-1094
31. Vuagniaux G, Vallet V, Jaeger NF, Pfister C, Bens M, Farman N, Courtois-Coutry N, Vandewalle A, Rossier BC, Hummler E: Activation of the amiloride-sensitive epithelial sodium channel by the serine protease mCAP1 expressed in a mouse cortical collecting duct cell line, J Am Soc Nephrol 2000, 11:828-834

32. Caldwell RA, Boucher RC, Stutts MJ: Serine protease activation of near-silent epithelial Na+ channels, Am J Physiol Cell Physiol 2004, 286:C190-194
33. Loffing J, Kaissling B: Sodium and calcium transport pathways along the mammalian distal nephron: from rabbit to human, Am J Physiol Renal Physiol 2003, 284:F628-643
34. Wang Q, Horisberger JD, Maillard M, Brunner HR, Rossier BC, Burnier M: Salt- and angiotensin II-dependent variations in amiloride-sensitive rectal potential difference in mice, Clinical and experimental pharmacology & physiology 2000, 27:60-66
35. Adachi M, Kitamura K, Miyoshi T, Narikiyo T, Iwashita K, Shiraishi N, Nonoguchi H, Tomita K: Activation of epithelial sodium channels by prostasin in Xenopus oocytes, J Am Soc Nephrol 2001, 12:1114-1121
36. Nikkari T: Comparative chemistry of sebum, J Invest Dermatol 1974, 62:257-267
37. Strauss JS, Pochi PE, Downing DT: The sebaceous glands: twenty-five years of progress, J Invest Dermatol 1976, 67:90-97
38. Falconer DS, Snell GD: TWO NEW HAIR MUTANTS, ROUGH AND FRIZZY: In The House Mouse. Edited by 1952, p. pp. 53-57
39. Herrmann T, van der Hoeven F, Grone HJ, Stewart AF, Langbein L, Kaiser I, Liebisch G, Gosch I, Buchkremer F, Drobnik W, Schmitz G, Stremmel W: Mice with targeted disruption of the fatty acid transport protein 4 (Fatp 4, Slc27a4) gene show features of lethal restrictive dermopathy, The Journal of cell biology 2003, 161:1105-1115
40. Koletzko S, Osterrieder S: Acute infectious diarrhea in children, Deutsches Arzteblatt international 2009, 106:539-547; quiz 548
41. Canessa CM, Merillat AM, Rossier BC: Membrane topology of the epithelial sodium channel in intact cells, The American journal of physiology 1994, 267:C1682-1690
42. List K, Haudenschild CC, Szabo R, Chen W, Wahl SM, Swaim W, Engelholm LH, Behrendt N, Bugge TH: Matriptase/MT-SP1 is required for postnatal survival, epidermal barrier function, hair follicle development, and thymic homeostasis, Oncogene 2002, 21:3765-3779
43. List K, Kosa P, Szabo R, Bey AL, Wang CB, Molinolo A, Bugge TH: Epithelial integrity is maintained by a matriptase-dependent proteolytic pathway, The American journal of pathology 2009, 175:1453-1463
44. List K, Hobson JP, Molinolo A, Bugge TH: Co-localization of the channel activating protease prostasin/(CAP1/PRSS8) with its candidate activator, matriptase, Journal of cellular physiology 2007, 213:237-245
45. Netzel-Arnett S, Currie BM, Szabo R, Lin C-Y, Chen L-M, Chai KX, Antalis TM, Bugge TH, List K: Evidence for a Matriptase-Prostasin Proteolytic Cascade Regulating Terminal Epidermal Differentiation, J Biol Chem 2006, 281:32941-32945

Table I

Inheritance of the *fr*, *Δ* and fr^{CR} mutations. Number of animals per genotype is indicated.

fr genotype	+/+	*fr*/+	Δ/+	*fr*/Δ	*fr*/*fr*
Breeding pairs					
fr/+ x Δ/+, n=111	42	32	30	7	-
Observed %	38	29	27	6	-
Expected %	25	25	25	25	-
χ^2 test	21.3 p<0.001				
fr/Δ x *fr*/+, n=95		40	28	12	15
Observed %	-	42	29	13	16
Expected %	-	25	25	25	25
χ^2 test	22.0 p<0.01				

$\boldsymbol{fr^{CR}}$ genotype	+/+	fr^{CR}/+	fr^{CR}/fr^{CR}
Breeding pairs			
fr^{CR}/+ x fr^{CR}/+, n=60	12	42	6
Observed %	20	70	10
Expected %	25	50	25
χ^2 test	18.0 p<0.01		
fr^{CR}/+ x fr^{CR}/fr^{CR}, n=50	-	32	18
Observed %	-	64	36
Expected %	-	50	50
χ^2 test	7.8 p<0.01		

A

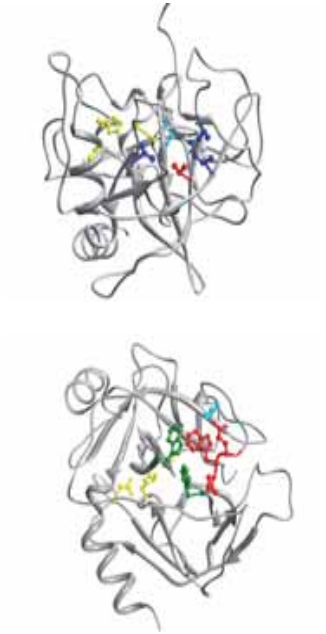

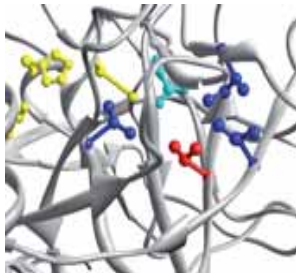

V170

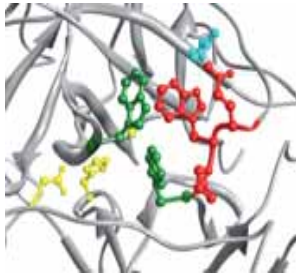

G54-P57

B

```
mouse   MALRVGLGLGQLEAVTILLLLGLLQSGIRADGTEASCGAVIQPRITGGGSAKPGQWPWQV 60
rat     MALRVGLGLGQLEALFILLLIGLLQSRIGADGTEASCGAVIQPRITGGGSAKPGQWPWQV 60
human   MAQKGVLGPGQLGAVAILLYLGLLRSGTGAEGAEAPCGVAPQARITGGSSAVAGQWPWQV 60
        ** :  ** *** *: *** :***:*   *:*:**.**.. *.*****.** .*******

                                  ↓
mouse   SITYDGNHVCGGSLVSNKWVVSAAHCFPREHSREAYEVKLGAHQLDSYSNDTVVHTVAQI 120
rat     SITYNGVHVCGGSLVSNQWVVSAAHCFPREHSKEEYEVKLGAHQLDSFSNDIVVHTVAQI 120
human   SITYEGVHVCGGSLVSEQWVLSAAHCFPSEHHKEAYEVKLGAHQLDSYSEDAKVSTLKDI 120
        ****:* *********::**:******* ** :* ************:*:*  * *: :*

                ↓
mouse   ITHSSYREEGSQGDIALIRLSSPVTFSRYIRPICLPAANASFPNGLHCTVTGWGHVAPSV 180
rat     ISHSSYREEGSQGDIALIRLSSPVTFSRYIRPICLPAANASFPNGLHCTVTGWGHVAPSV 180
human   IPHPSYLQEGSQGDIALLQLSRPITFSRYIRPICLPAANASFPNGLHCTVTGWGHVAPSV 180
        *.*.** :*********::** *:************************************

                                                                   ↓
mouse   SLQTPRPLQQLEVPLISRETCSCLYNINAVPEEPHTIQQDMLCAGYVKGGKDACQGDSGG 240
rat     SLQTPRPLQQLEVPLISRETCSCLYNINAVPEEPHTIQQDMLCAGYVKGGKDACQGDSGG 240
human   SLLTPKPLQQLEVPLISRETCNCLYNIDAKPEEPHFVQEDMVCAGYVEGGKDACQGDSGG 240
        ** **:***************.*****:* ***** :*:**:******:************

mouse   PLSCPMEGIWYLAGIVSWGDACGAPNRPGVYTLTSTYASWIHHHVAELQPRVVPQTQESQ 300
rat     PLSCPIDGLWYLAGIVSWGDACGAPNRPGVYTLTSTYASWIHHHVAELQPRAVPQTQESQ 300
human   PLSCPVEGLWYLTGIVSWGDACGARNRPGVYTLASSYASWIQSKVTELQPRVVPQTQESQ 300
        *****::*:***:*********** ********:*:*****: :*:******.********

mouse   PDGHLCNHHPVFSSAAAPKLLRPVLFLPLGLTLGLLSLA---- 339
rat     PDGHLCNHHPVFNLAAAQKLSRPILFLPLSLTLGLFSLWLEH- 342
human   PDSNLCGSHLAFSSAPAQGLLRPILFLPLGLALGLLSPWLSEH 343
        **.:**. * .*. *.*  * **:*****.*:***:*
```

Fig. 1

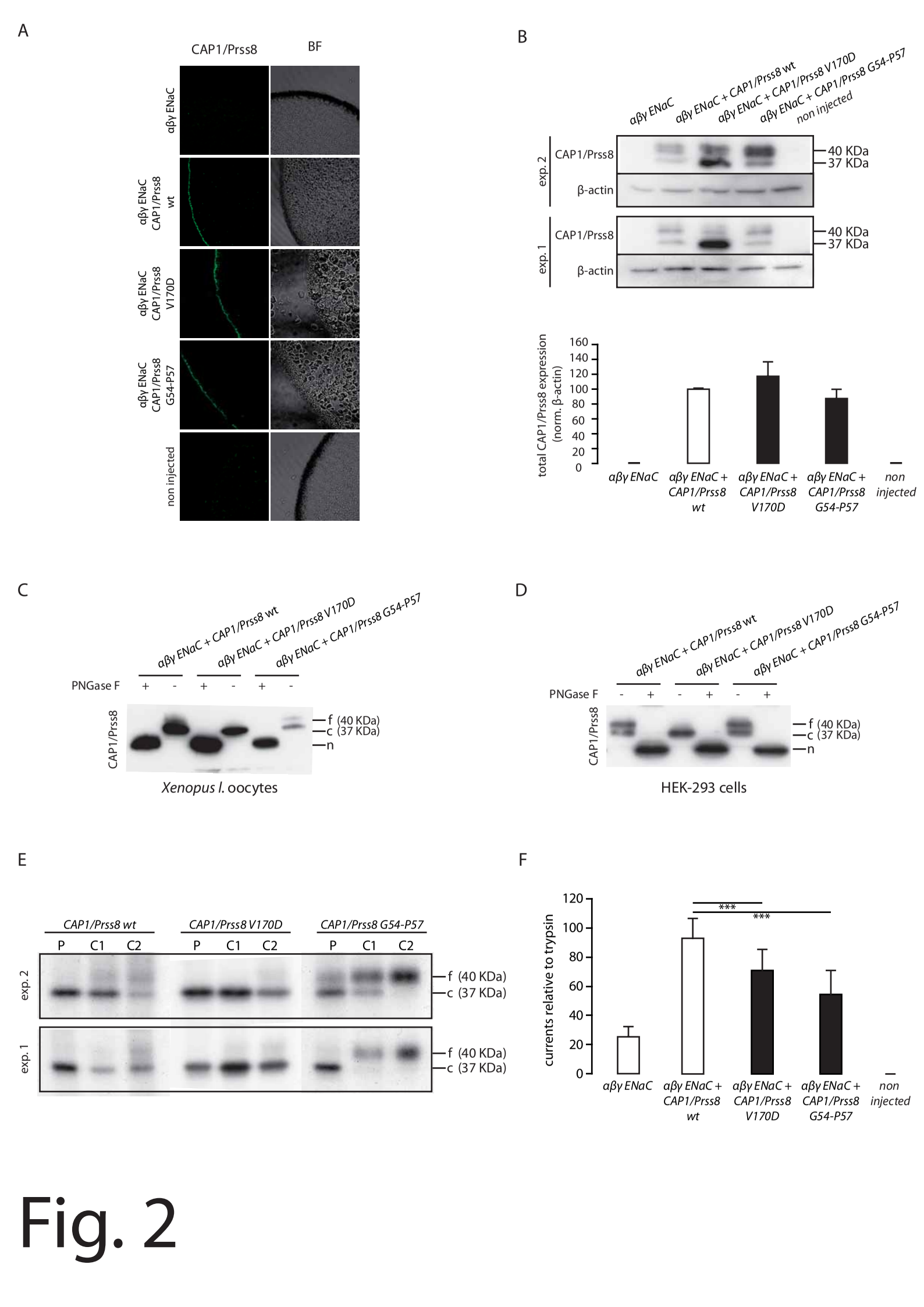
A
CAP1/Prss8
BF
αβγ ENaC
αβγ ENaC CAP1/Prss8 wt
αβγ ENaC CAP1/Prss8 V170D
αβγ ENaC CAP1/Prss8 G54-P57
non injected
B
αβγ ENaC
αβγ ENaC + CAP1/Prss8 wt
αβγ ENaC + CAP1/Prss8 V170D
αβγ ENaC + CAP1/Prss8 G54-P57
non injected
exp. 2
CAP1/Prss8
β-actin
40 KDa
37 KDa
exp. 1
CAP1/Prss8
β-actin
40 KDa
37 KDa
total CAP1/Prss8 expression (norm. β-actin)
160
140
120
100
80
60
40
20
0
αβγ ENaC
αβγ ENaC + CAP1/Prss8 wt
αβγ ENaC + CAP1/Prss8 V170D
αβγ ENaC + CAP1/Prss8 G54-P57
non injected
C
αβγ ENaC + CAP1/Prss8 wt
αβγ ENaC + CAP1/Prss8 V170D
αβγ ENaC + CAP1/Prss8 G54-P57
PNGase F
+ - + - + -
CAP1/Prss8
f (40 KDa)
c (37 KDa)
n
Xenopus l. oocytes
D
αβγ ENaC + CAP1/Prss8 wt
αβγ ENaC + CAP1/Prss8 V170D
αβγ ENaC + CAP1/Prss8 G54-P57
PNGase F
- + - + - +
CAP1/Prss8
f (40 KDa)
c (37 KDa)
n
HEK-293 cells
E
CAP1/Prss8 wt
CAP1/Prss8 V170D
CAP1/Prss8 G54-P57
P C1 C2 P C1 C2 P C1 C2
exp. 2
f (40 KDa)
c (37 KDa)
exp. 1
f (40 KDa)
c (37 KDa)
F
currents relative to trypsin
120
100
80
60
40
20
0
***
***
αβγ ENaC
αβγ ENaC + CAP1/Prss8 wt
αβγ ENaC + CAP1/Prss8 V170D
αβγ ENaC + CAP1/Prss8 G54-P57
non injected

Fig. 2

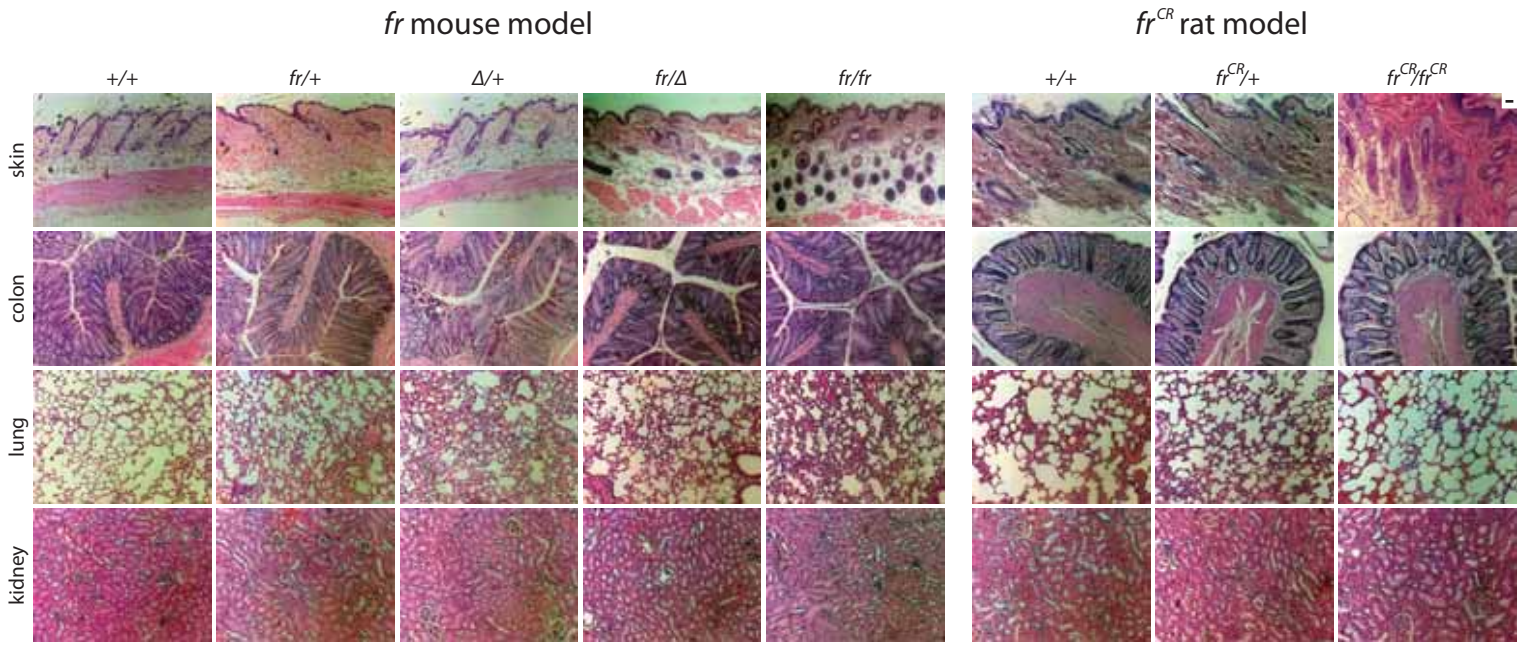
fr mouse model
fr^{CR} rat model
+/+
fr/+
Δ/+
fr/*Δ*
fr/*fr*
+/+
fr^{CR}/+
fr^{CR}/*fr*^{CR}
skin
colon
lung
kidney

Fig. 3

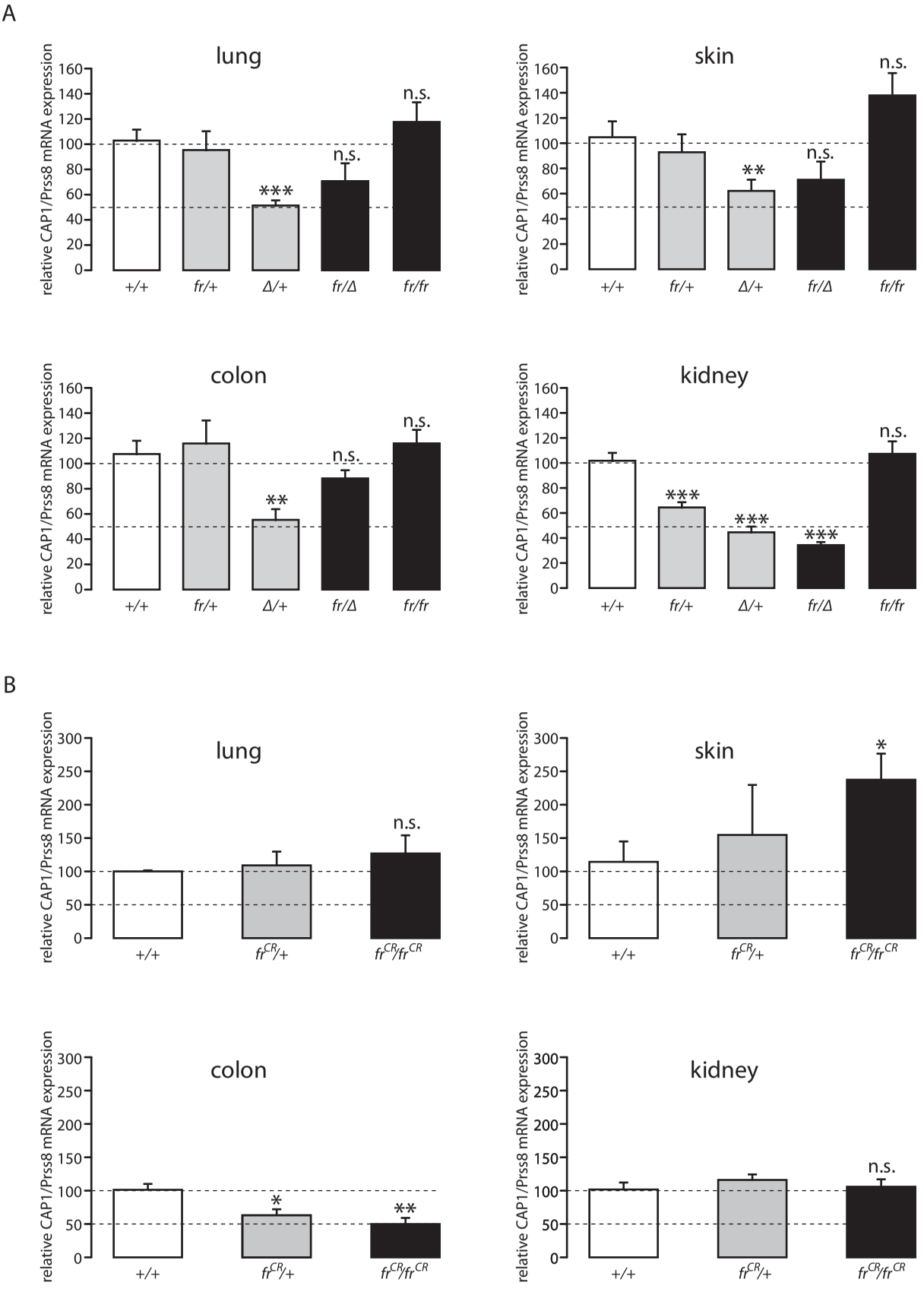
A
lung
skin
colon
kidney
relative CAP1/Prss8 mRNA expression
+/+
fr/+
Δ/+
fr/Δ
fr/fr
n.s.
***
**
B
$fr^{CR}/+$
fr^{CR}/fr^{CR}
*

Fig. 4

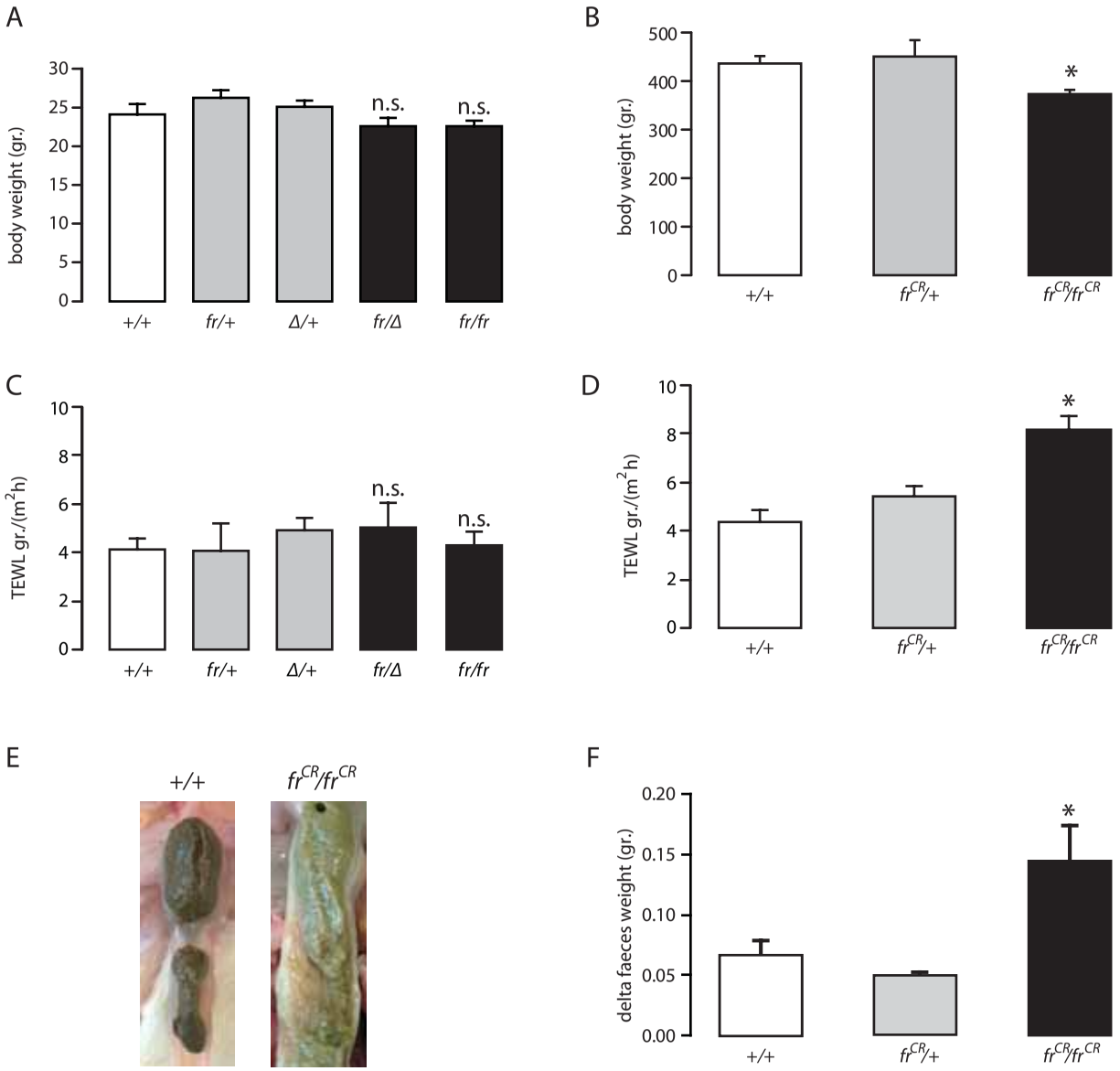
A
body weight (gr.)
30
25
20
15
10
5
0
n.s.
n.s.
+/+
fr/+
Δ/+
fr/Δ
fr/fr
B
body weight (gr.)
500
400
300
200
100
0
*
+/+
fr^CR/+
fr^CR/fr^CR
C
TEWL gr./(m^2h)
10
8
6
4
2
0
n.s.
n.s.
+/+
fr/+
Δ/+
fr/Δ
fr/fr
D
TEWL gr./(m^2h)
10
8
6
4
2
0
*
+/+
fr^CR/+
fr^CR/fr^CR
E
+/+
fr^CR/fr^CR
F
delta faeces weight (gr.)
0.20
0.15
0.10
0.05
0.00
*
+/+
fr^CR/+
fr^CR/fr^CR

Fig. 5

A

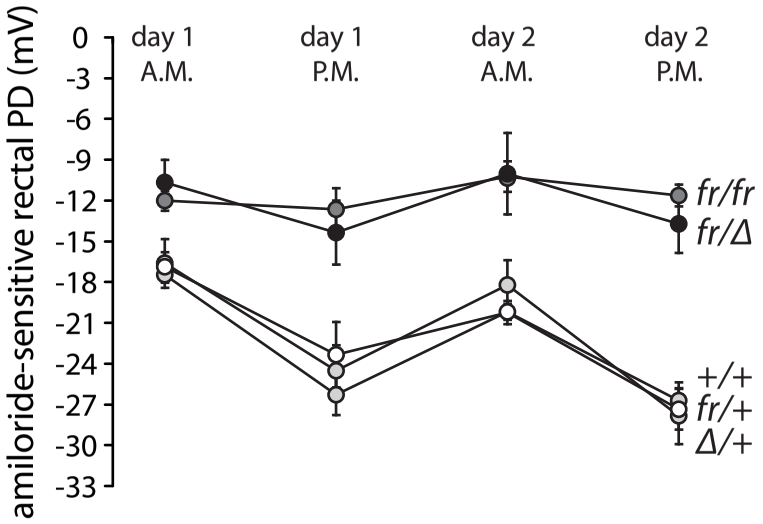
amiloride-sensitive rectal PD (mV)
0
-3
-6
-9
-12
-15
-18
-21
-24
-27
-30
-33
day 1
A.M.
day 1
P.M.
day 2
A.M.
day 2
P.M.
fr/fr
fr/Δ
+/+
fr/+
Δ/+

B

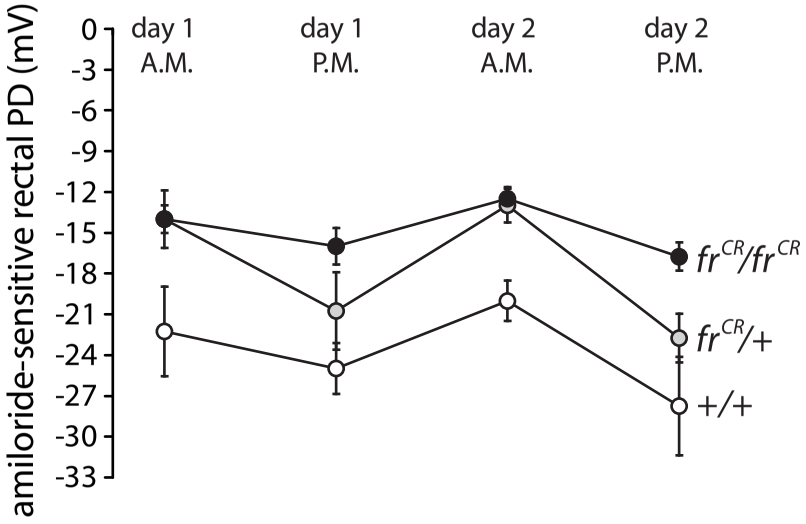
amiloride-sensitive rectal PD (mV)
0
-3
-6
-9
-12
-15
-18
-21
-24
-27
-30
-33
day 1
A.M.
day 1
P.M.
day 2
A.M.
day 2
P.M.
frCR/frCR
frCR/+
+/+

Fig. 6